ISA Transactions 58 (2015) 586–594

Contents lists available at ScienceDirect

ISA Transactions

journal homepage: www.elsevier.com/locate/isatrans

Implementation of fuzzy-sliding mode based control of a grid connected photovoltaic system

Abdelkrim Menadi [a,*], Sabrina Abdeddaim [b], Ahmed Ghamri [b], Achour Betka [b]

[a] Laboratoire LMSE, Electrical Engineering Department, University of Biskra, Algeria
[b] Laboratoire LGEB, Electrical Engineering Department, University of Biskra, Algeria

ARTICLE INFO

Article history:
Received 7 January 2015
Received in revised form
26 May 2015
Accepted 11 June 2015
Available online 1 August 2015
This paper was recommended for publication by Dr. Jeff Pieper

Keywords:
Photovoltaic
Grid connected
MPPT
Sliding mode control
Fuzzy logic
Unity power factor

ABSTRACT

The present work describes an optimal operation of a small scale photovoltaic system connected to a micro-grid, based on both sliding mode and fuzzy logic control. Real time implementation is done through a dSPACE 1104 single board, controlling a boost chopper on the PV array side and a voltage source inverter (VSI) on the grid side. The sliding mode controller tracks permanently the maximum power of the PV array regardless of atmospheric condition variations, while The fuzzy logic controller (FLC) regulates the DC-link voltage, and ensures via current control of the VSI a quasi-total transit of the extracted PV power to the grid under a unity power factor operation. Simulation results, carried out via Matlab–Simulink package were approved through experiment, showing the effectiveness of the proposed control techniques.

1. Introduction

As conventional energy sources are vanishing fast with a consequent rise in cost, considerable attention is being paid to other alternative sources. Nowadays, solar energy, which is free and abundant in most parts of the world, has proven to be an economical source of energy in many applications. Nowadays, grid connected PV systems have acquired a mature technology, and is receiving more attention in recent years as decentralized sources, to share the power demand in case of grid disturbances, improving therefore the stability of the interconnected networks. In this topic, various studies have been carried out on sizing [1,2], matching [3], and optimizing [4]. Different optimization strategies were proposed to improve the overall system efficiency, by extracting and then injecting the maximum PV power into the grid. The first task deals with tracking the maximum power point (MPP) of the PV array, where many algorithms are used; whereas, the second task consists in injecting this power with minimum losses. As exposed in [5,6], the conventional Perturb & Observe (PO) method does not provide a good accuracy and response time, since oscillation occurs around the optimal point in steady state [7]. To overcome this drawback, several intelligent and complex control methods, such as fuzzy logic [8,9] genetic algorithms [10,11], neural network [12], neuro-fuzzy MPPT strategies [13], were developed in recent years to improve accuracy and response time.

Compared to the classical algorithms, artificial techniques proved a notable superiority, since the maximum power point is always tracked very fast regardless any sudden changes of solar insolation, and without oscillation in steady state [14]. As an interface with the AC side, two or multi-level VSI with various pulse width modulation techniques, are currently in use. They are controlled either in current or voltage mode to allow the PV power flow of the PV power to the utility under a controlled power factor operation.

In this scope, the present paper describes how an operation of a small scale PV system connected to a microgrid can be achieved. The main tasks assigned to the proposed control strategies are

1. A permanent tracking of the maximum power point of the PV array, by a proper tuning of the boost chopper duty cycle, using sliding mode based MPPT control.
2. A total flow of the extracted PV power to the utility, via current control of the VSI, under a unity power factor operation.

In order to investigate the system performances, and prior to numerical simulation, each part of the system is modeled, taking into account the following assumptions: the synchronization of the PV system with the grid is not considered in this study, power converters

* Correspondence to: Laboratoire LGEB, Electrical Engineering Department, University of Biskra, Algeria. Tel.: +213 665150341.
E-mail addresses: a.menadi@univ-biskra.dz (A. Menadi), s_abdeddaim@yahoo.fr (S. Abdeddaim), ghamri65@gmail.com (A. Ghamri), betkaachour@gmail.com (A. Betka).

http://dx.doi.org/10.1016/j.isatra.2015.06.009
0019-0578/

Nomenclature

V_{PV}	photovoltaic array voltage (V)
I_{PV}	photovoltaic array current (A)
I_{sc}	photovoltaic short circuit (A)
I_o	inverse saturation current (A)
V_{oc}	PV open circuit voltage (V)
V_{th}	thermal voltage (V)
R_s	array series resistance (Ω)
α	chopper duty cycle
σ	sliding surface
ΔT	temperature variation
V_{DC}, V_{DCref}	actual and reference DC link voltage (V)
E, E_r	actual and reference insolation (W/m²)
I_a, I_b, I_c	grid currents (A)
e_a, e_b, e_c	grid voltages (V)
V_a, V_b, V_c	inverter output voltages (V)
θ	grid estimated angle (rad)
FLC	fuzzy logic controller
I, I_r	actual and reference current (A)
V, V_r	actual and reference voltage (V)
β, γ	current and voltage change coefficient depending on the temperature

are supposed lossless. Thus, the paper is organized as follows: Section 2 shows the modeling of different system components, while in Section 3, the proposed control strategies are presented. To test the effectiveness of these techniques, Section 4 illustrates both the practical and simulation results. Section 5 concludes this work.

2. System description and modeling

The synoptic schematic of the studied system is shown in Fig. 1. The first stage of the conversion chain is composed of a PV array and a boost DC–DC converter, which rises the relatively low optimum solar voltage into a suitable DC link value. The second stage is composed of a three phase voltage source inverter connected to the grid via an inductive filter and a step up transformer.

2.1. PV array modeling

Photovoltaic arrays are neither voltage nor current sources, but can be approximated as current generators with dependent voltage sources, where the I–V characteristic can be expressed by an implicit Eq. [15]:

$$I_{PV} = I_{sc} - I_0\left[\exp\left(\frac{V_{PV}+R_s\,I_{PV}}{V_{th}}\right)-1\right] \tag{1}$$

I–V curve is crucially influenced by solar insolation and temperature variations. The adaption of Eq. (1) to different levels of these inputs can be handled by the following equations:

$$\Delta I = \beta\left(\frac{E}{E_r}\right)\Delta T + \left(\frac{E}{E_r}-1\right)I_{sc} \tag{2}$$

$$\Delta V = \gamma\Delta T - R_s\Delta I \tag{3}$$

$$V = V_r + \Delta V \tag{4}$$

$$I = I_r + \Delta I \tag{5}$$

2.2. DC–DC converter model

To test the control techniques on continuous dynamic systems, the state space average models of power converters are generally used, neutralizing so the system's discontinuity caused by the switching phenomena. Referring to Fig. 2, the continuous dynamic model of the boost DC–DC converter is obtained through the combination of the switching modes, as follows:

For $S=0$, the following expressions are deduced for storage elements L_1 and C:

$$L_1\frac{di_{L1}}{dt} = V_{PV} - V_{DC} \tag{6}$$

$$C\frac{dV_{DC}}{dt} = i_{L1} - \frac{V_{DC}}{R_L} \tag{7}$$

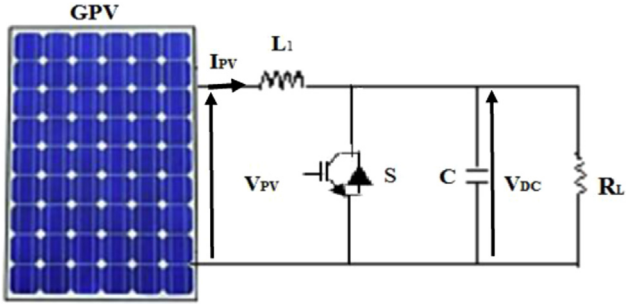

Fig. 2. DC–DC boost converter schematic.

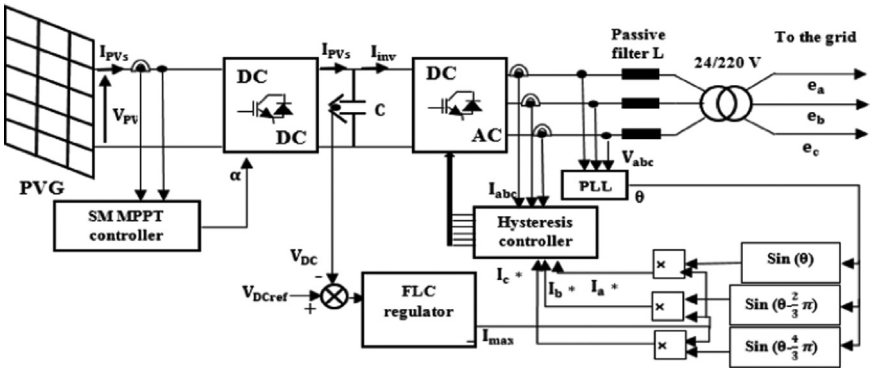

Fig. 1. Synoptic of the grid connected PV system.

For $S=1$, these differential equations are expressed as

$$L_1\frac{di_{L1}}{dt}=V_{PV} \tag{8}$$

$$C\frac{dV_{DC}}{dt}=i_C \tag{9}$$

R_L denotes the system's equivalent load at the DC side.

The two equation sets (6,7) and (8,9) are weighted by the duty ratio α and added to get the average state space model of the converter [15]

$$\dot{x}=\begin{bmatrix}0 & -\frac{1-\alpha}{L_1}\\ -\frac{1-\alpha}{C} & -\frac{1}{R_LC}\end{bmatrix}x+\begin{bmatrix}\frac{1}{L_1}\\ 0\end{bmatrix}V_{PV} \tag{10}$$

where

$$x=\begin{bmatrix}I_{L1}\\ V_{DC}\end{bmatrix}$$

2.3. Voltage source inverter model

The DC–AC converter is a three phase two level voltage source inverter, controlled by the hysteresis current strategy. The inverter's output voltages (V_a, V_b, V_c) as well as the inverter current on the DC side I_{inv} are related to the switching states K_1, K_2 and K_3 by the following expression [16]:

$$\begin{bmatrix}V_a\\ V_b\\ V_c\end{bmatrix}=\frac{V_{DC}}{3}\begin{bmatrix}2 & -1 & -1\\ -1 & 2 & -1\\ -1 & -1 & 2\end{bmatrix}\begin{bmatrix}K_1\\ K_2\\ K_3\end{bmatrix} \tag{11}$$

$$I_{inv}=K_1i_a+K_2i_b+K_3i_c \tag{12}$$

2.4. Grid model

The dynamic model of the grid on the low voltage side of the step up transformer is obtained via a simple addition of both no-load voltages e_a, e_b, e_c and voltages across the inductive filters [17]:

$$\begin{cases}V_a=I_a*R+L*\frac{dI_a}{dt}+e_a\\ V_b=I_b*R+L*\frac{dI_b}{dt}+e_b\\ V_c=I_c*R+L*\frac{dI_c}{dt}+e_c\end{cases} \tag{13}$$

3. Control approaches

3.1. PV side control

3.1.1. Sliding mode MPPT controller

Recently, sliding mode control became more attractive for MPP tracking using Microcontrollers. It presents notable robustness in disturbance rejection, and good performances for optimum point tracking. In this work, a first order sliding mode controller is adopted as the optimization tool. The concept of the approach can be introduced by selecting the sliding surface σ, defined as the incremental conductance condition to extract the maximum power:

$$\sigma=\frac{dI_{pv}}{dV_{pv}}V_{pv}+I_{pv} \tag{14}$$

Based on the observation of the operation region shown in Fig. 5, the duty cycle α can be increased or decreased with a preset increment Δ as a result of the surface sign to approach the optimal point MPP:

$$\alpha_{update}=\begin{cases}\alpha+\Delta & \text{for } \sigma>0\\ \alpha-\Delta & \text{for } \sigma<0\end{cases} \tag{15}$$

The structure of the sliding mode control consists of two parts: the first one deals with the equivalent control quantity α_{eq}, and the second one provides the stabilization part α_n:

$$\alpha=\alpha_{eq}+\alpha_n \tag{16}$$

α_{eq} is derived from the condition $\dot{\sigma}=0$, providing the conventional duty-cycle in steady state [18]:

$$\alpha_{eq}=1-\frac{V_{pv}}{V_{DC}} \tag{17}$$

The stabilization part α_n is considered as the required effort to join the condition $\sigma=0$ once the system's control starts. The existence of the approaching mode can be guaranteed using direct Lyapounov stability theorem, as follows:

One can define a quadratic positive function related to the sliding surface:

$$v=\frac{1}{2}*\sigma^2 \tag{18}$$

Hence, the gradient of the cost function V is derived as

$$\dot{v}=\dot{\sigma}\sigma \tag{19}$$

The achievement of $\sigma=0$ is obtained if Eq. (19) is kept negative semi-definite ($\dot{\sigma}\sigma\leq 0$). Soltine in [19] proposes the stabilization part of the control α_n as a linear function of the sliding surface σ, which permits to attract the sliding surface and to soften the operating point at its optimum:

$$\alpha_n=-K\cdot\sigma \tag{20}$$

Since the range of the duty cycle must lie in $0<\alpha<1$, the real control signal is proposed as

$$\alpha=\begin{cases}1 & \text{for} \quad \alpha\geq 1\\ \alpha_{eq}-K\sigma & for \quad 0<\alpha<1\\ 0 & \text{for} \quad \alpha\leq 0\end{cases} \tag{21}$$

The continuous variation of the duty cycle in the specified range can be ensured without violation if the scaling constant K is not selected too large: chosen as the inverse of the maximum equivalent load on the DC side: $K\leqslant 1/|R_L|_{max}$,[20]; where $|R_L|_{max}$ is quantified on the basis of a threshold optimal PV power P_{min} extracted after sunrise, a power conversion on both the DC–DC converter sides, and a quite regulation of the DC link voltage, as follows:

$$R_L|_{\max}=\frac{V_{DCref}^2}{P_{\min}}$$

3.2. Grid side control

To permit a total flow of the extracted power into the grid, the voltage source inverter control is performed in a cascade manner through the control of both the DC link voltage and the grid currents, leading so to a unit power factor functioning.

3.2.1. DC link voltage controller

To maintain a constant DC link voltage at a reference value regardless the system's disturbances, a fuzzy logic controller is chosen. Before performing the controller design, the tuning freedom degree is first chosen:

The dynamic equation of the DC link voltage, given in Eq. (7), is rewritten as [21]

$$C\frac{dV_{DC}}{dt}=I_{PVs}-I_{inv} \tag{22}$$

The regulation of the DC link voltage is carried out by the inverter current I_{inv} on the DC side, whereas I_{pvs}, reflecting atmospheric variations, must be rejected by the controller.

The design of the FLC controller passes through the set of four conventional steps: fuzzification, rule bases, fuzzy inference and defuzzification, as shown in Fig. 3; where the tracking error e and its derivative Δe, sensed at two sampling time k and $(k-1)$ are respectively defined as

$$e = V_{DC} - V_{DCref} \tag{23}$$

$$\Delta e = e(k) - e(k-1) \tag{24}$$

To obtain good tracking performances (accuracy and response time) in the case of large disturbance variation, 49 fuzzy rules, with the following linguistic variables, were chosen:

NB: Negative Big, NM: Negative Medium, NS: Negative Small, ZE: Zero, PS: Positive Small, PM: Positive Medium, PB: Positive Big.

Furthermore, to avoid hard calculation, triangle membership functions are chosen for both input and output as depicted in Fig. 4.

The inverter current I_{inv} will be increased or decreased in the positive or in the negative direction with a small or a large value until the DC voltage approximates its reference, and the tracking error almost equals zero.

The fuzzy inference step is carried out by Mamdani's method (Table 1), whereas the defuzzification uses the center of gravity technique to compute the DC side inverter current [22]:

$$I_{inv} = \frac{\sum_{i=1}^{n}(dI_{inv}^{*}u_i)}{\sum_{i=1}^{n}u_i} \tag{25}$$

Finally, the three normalization gains K_{11}, K_{12} allow to convert the real input values into fuzzy quantities and K_{13} provides the real value of the output fuzzy amount.

3.2.2. Inverter current control

The VSI control is achieved in current mode using simple hysteresis controllers; where the measured grid currents I_a, I_b, I_c match their references according to a preset hysteresis band Δi. Firstly, the reference current peak value I_{max} and the grid angle θ are deduced before the inverter switching starts.

Assuming an operation with a unit power factor in the grid side, the peak value of the AC current I_{max} is related to I_{inv} through the following linear equation:

$$I_{inv} = K_c^{*} I_{\max} \tag{26}$$

where K_c is computed on the basis of a lossless inverter [23]:

$$K_c = \frac{\sqrt{3}}{\sqrt{2}}\frac{V_{rms}}{V_{DCref}} \tag{27}$$

To achieve synchronization with the grid, a phased locked loop (PLL) is used. It provides, in real time, the grid phase θ and frequency on the basis of grid voltage orientation on the q-axis ($V_{rd}=0$ and $V_{rq} = -\sqrt{3}V_{rms}$)[24].

The amplitude of the reference current I_{max} takes care of the active power demand on the grid side. Thus, the switching signals of the inverter are obtained by comparing the measured grid currents (I_a, I_b, I_c) with their reference quantities (I_a^{*}, I_b^{*}, I_c^{*}) using Schmidt triggers.

4. Obtained results

4.1. Simulation results

The effectiveness of the proposed control strategies are firstly checked through numerical simulation on MATLAB/Simulink package, and undertaken on the system given in appendix. The solar insolation level, considered as the system input is varied with 200 W/m² steps over a time span of 10 s, whereas the temperature is kept constant at 25 °C, as shown in Fig. 7.

Figs. 8 and 9 show the PV array current and power respectively, plotted together with the off-line optimum quantities. One can notice that

1- The PV array current and power reach the optimum theoretical values ($I_{op\text{-}ref}$, $P_{op\text{-}ref}$) within milliseconds despite solar insolation variations, which consequently prove the ability of the

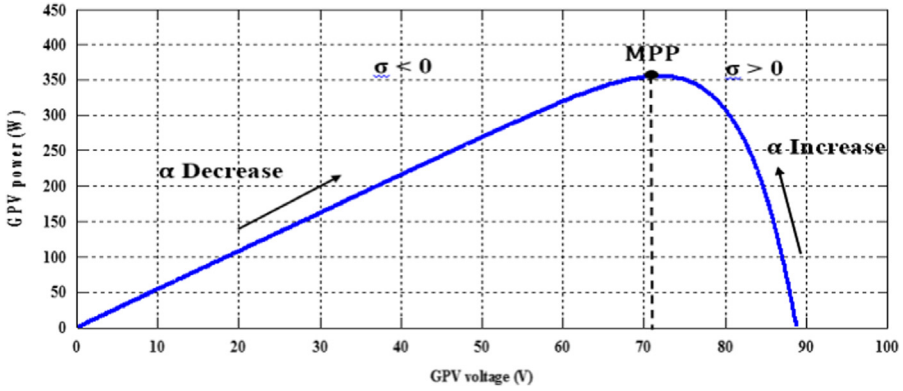

Fig. 3. Duty cycle tuning.

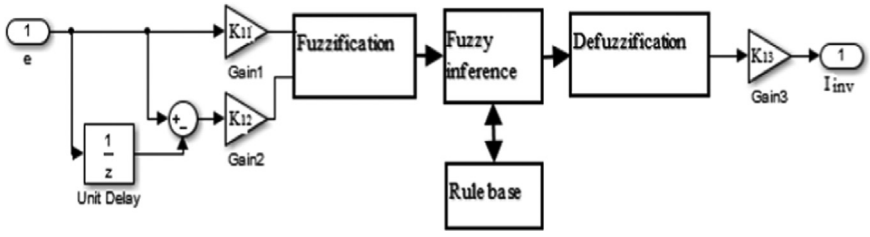

Fig. 4. FLC DC link voltage controller.

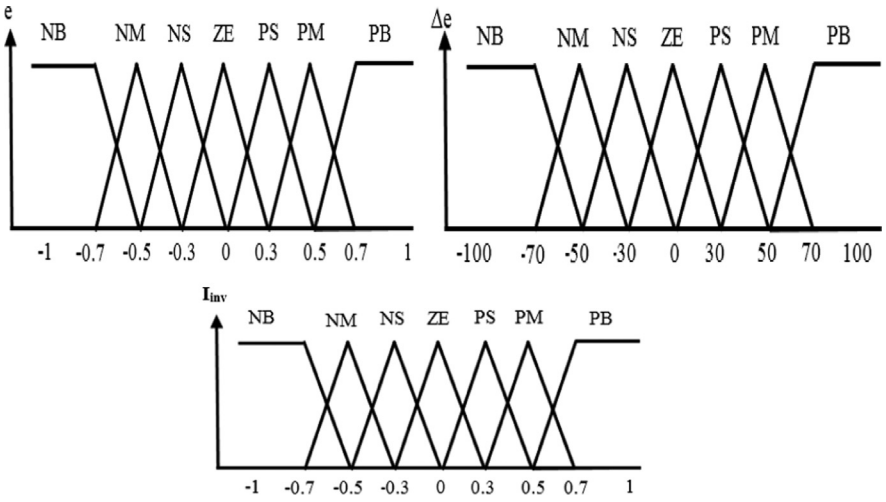

Fig. 5. Membership functions of the input and the output.

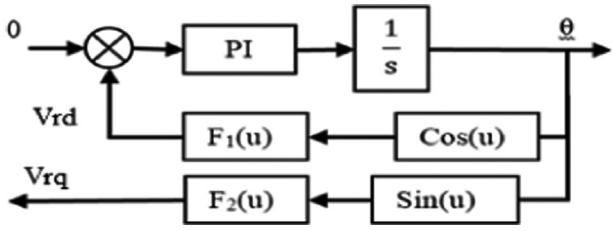

Fig. 6. Phase locked loop (PLL) schematic.

Table 1
Rule base for the DC link voltage controller.

e							
Δ*e*	NB	NM	NS	ZE	PS	PM	PB
NB	NB	NB	NB	NB	NM	NS	ZE
NM	NB	NB	NB	NM	NS	ZE	PS
NS	NB	NB	NM	NS	ZE	PS	PM
ZE	NB	NM	NS	ZE	PS	PM	PB
PS	NM	NS	ZE	PS	PM	PB	PB
PM	NS	ZE	PS	PM	PB	PB	PB
PB	ZE	PS	PM	PB	PB	PB	PB

introduced sliding mode based MPPT to maintain the output at the optimal point with less chattering phenomena.

2- The current and power amounts increase proportionally with solar insolation, since the PV voltage is less affected by the insolation variation than the current.

Fig. 10 shows the DC link voltage regulation, with a step changing of the reference value from 150 V to 200 V at $t=2$ s. As can be seen, the measured voltage V_{DC} perfectly matches the reference profile in few milliseconds and without any overshoot. To check the speed of the transient step, the following performance index I_1 is quantified as

$$I_1 = \int |e(t)|dt \tag{28}$$

The small obtained surface ($I_1=2.182$) proves consequently that the fuzzy logic controller is fast.

Finally, in Fig. 11 is illustrated a sample of the grid voltage, reference and measured current curves. One notices that the hysteresis controller demonstrates notable tracking skills, since both the phase current and its reference are closely superposed. Furthermore, the quasi-totality of the PV energy is injected as active power into the grid, while the phase voltage and current are kept in phase, leading so to a unity power factor operation.

4.2. Experimental validation

To validate practically the numerical results, a test rig was built in the LGEB laboratory, where the PV array consists of two 175 Wp PV modules, connected in parallel and fixed on the roof. The boost chopper is composed of one IGBT module, switched at 15 kHz, and the voltage source inverter is a didactic three phase Semikron converter, with a common capacitive DC link. The inverter is connected to the utility via a passive filter and a step up 24/220 V transformer. The control algorithm is implemented with a dSPACE 1104 board from Texas Instrument with a TMS320F240 DSP (20 MHz).

The connection between the dSPACE board and the power converters is carried out by an interface card, which adapts the control signal levels to the IGBT's driver voltage. The different currents and voltages are obtained by the (LA25NP) and (LV25P) sensors, as depicted in Fig. 12. The experiment was conducted in a clear day, on the 9th of November 2014, where the solar insolation varies very slowly.

Figs 13 and 14 show the sliding mode based MPPT performances, where the PV array voltage and current curves are shown. Firstly, the PV array was kept disconnected from the system and the VS inverter current control is allowed. The PV generator current remains equal to zero until point A. At this moment, the sliding mode algorithm is compiled. As can be seen, the PV operating point (current, voltage) moves towards the optimum MPP zone (point B) with small oscillation, since the incremental conductance condition of the PV array $((dIpv/dVpv)V_{pv}+I_{pv})$ remains near zero, as shown in Fig. 13.

In order to check the robustness of the proposed MPPT controller in variable atmospheric conditions, a PV array emulator based on a controlled DC supply was built and introduced in the power system. This manner of emulating is flexible since it allows to change easily the solar irradiance profile. In Fig. 15 is displayed the experimental extracted PV power curve, obtained under randomly 200 W/m² step changes of the solar insolation (1000 W/m², 600 W/m², 400 W/m², 800 W/m², 1000 W/m²). As can be seen, once the control routine is enabled in point A, the operating points match the theoretical optimal values, with no oscillation observed around the MPP point. To emphasize on this controller skill, in Fig. 16 is shown the spectral analysis of the PV power in steady state. As observed, contrary to the conventional Perturb & Observe method, the fundamental harmonic

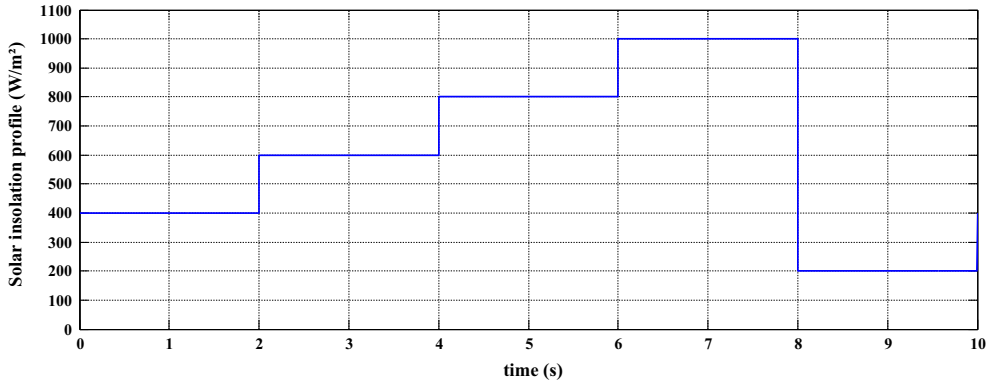

Fig. 7. Solar insolation profile.

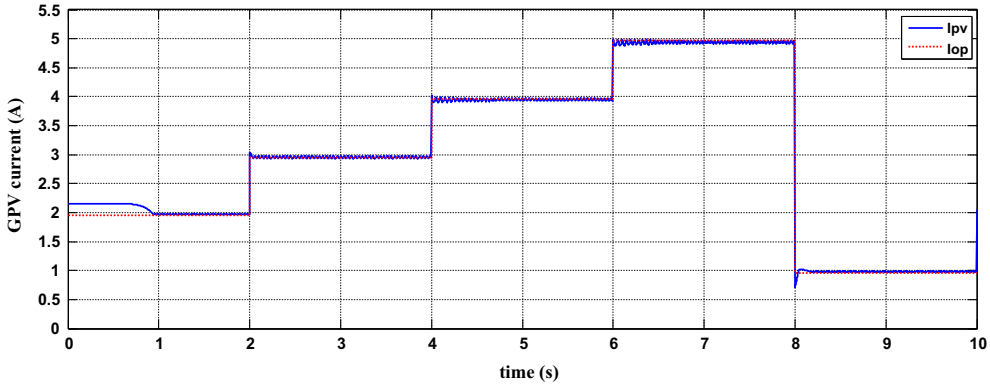

Fig. 8. PV array current curve.

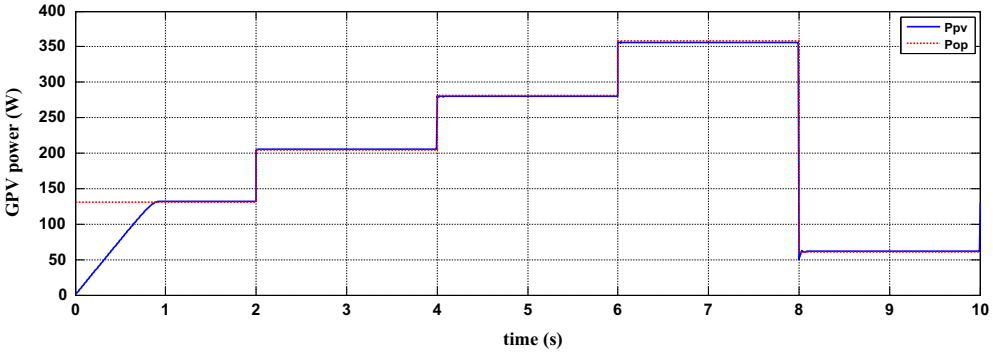

Fig. 9. PV array power curve.

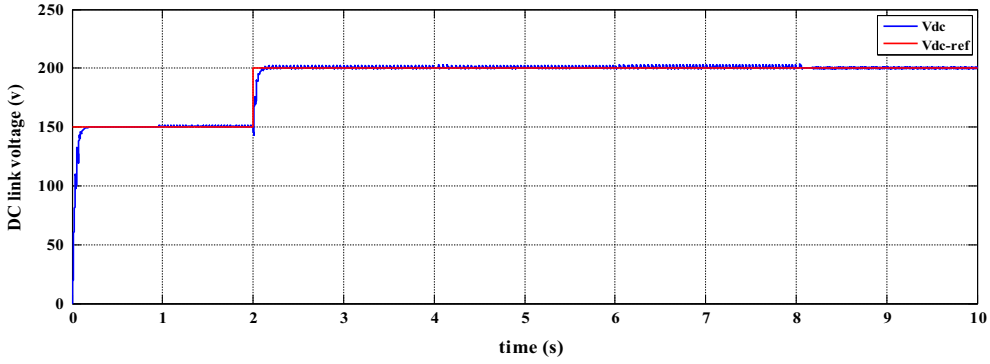

Fig. 10. DC link voltage curve.

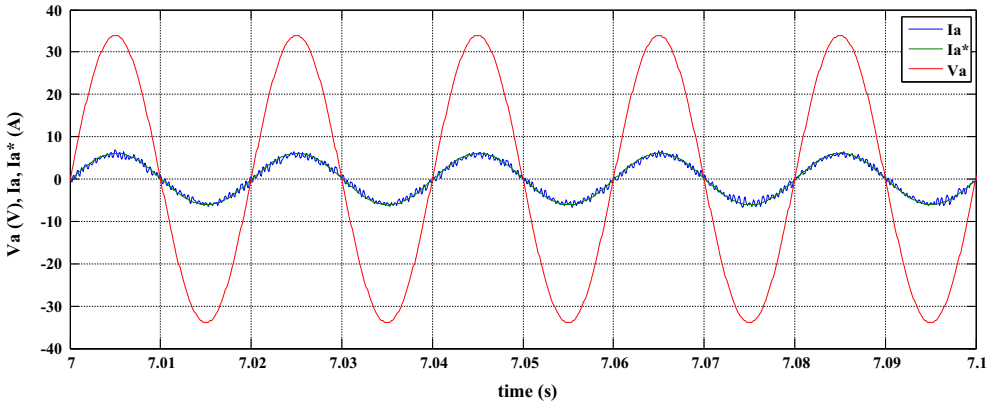

Fig. 11. Phase voltage, measured and reference current curves.

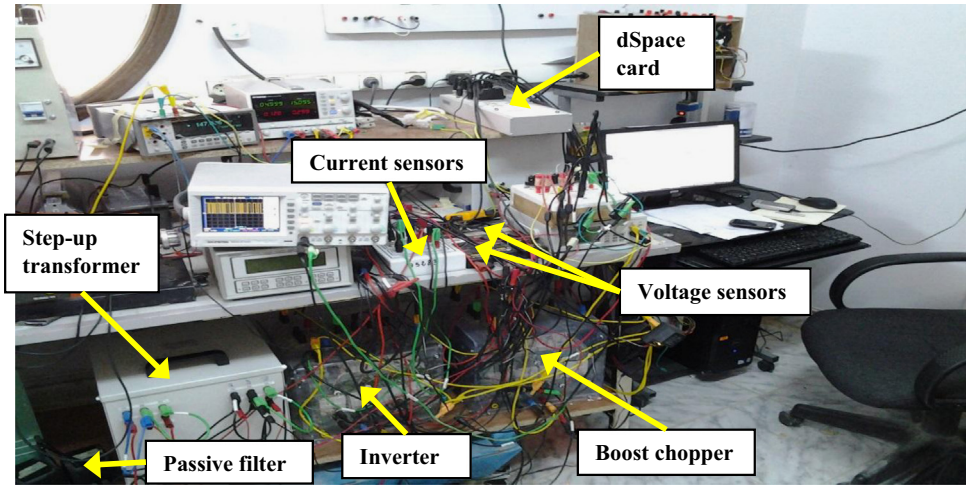

Fig. 12. Experimental test bench.

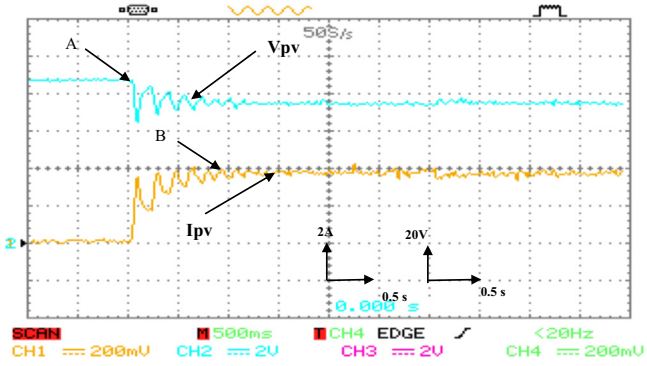

Fig. 13. PV voltage and current curves.

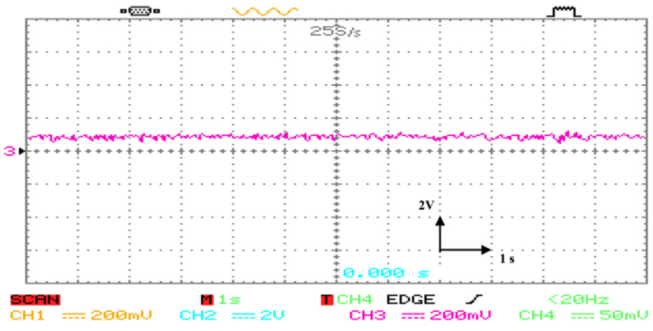

Fig. 14. Accuracy of the MPPT controller.

dominates the curve with no noticeable low frequencies, reflecting the oscillation in steady state is distinguished.

Fig. 17 shows the shape of the DC-link voltage, where a step change of the reference value was applied at $t = 0.23$ s (from 150 V to 200 V). As can be seen, the same performances obtained numerically are reproduced, and the DC voltage tracking is perfect.

To check the DC bus regulation performances in a comparative way, in Fig. 18 is plotted the DC voltage curve using a PI based control. As can be seen, the settling time observed in Fig. 17 is shorter than the time computed in Fig. 18. This situation can be explained by the fact that in case of the PI controller, the grid peak current computed in Eq. (29) as the control input is affected by the PV side dynamics (I_{pvs}), contrary to the fuzzy based control, which adapts the control input via the rule table. In addition, the selection of controller gains is usually

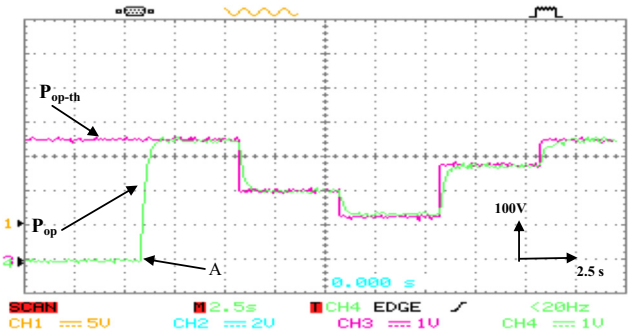

Fig. 15. PV power curve under insolation variations.

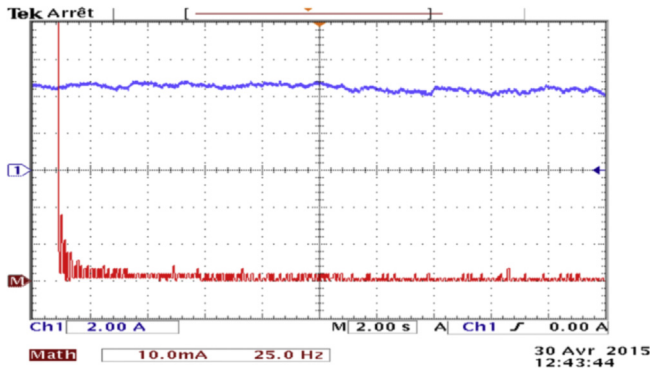

Fig. 16. PV power spectral curve.

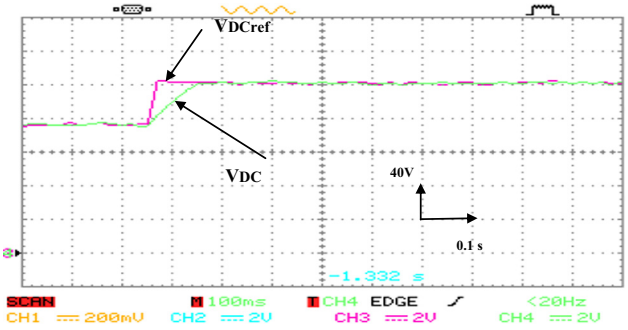

Fig. 17. The DC-link voltage curve with FLC.

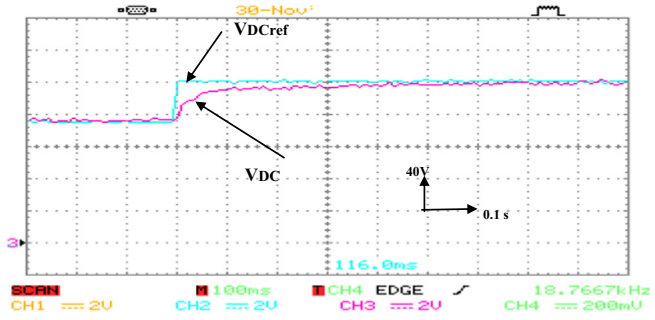

Fig. 18. The DC-link voltage curve with PI controller.

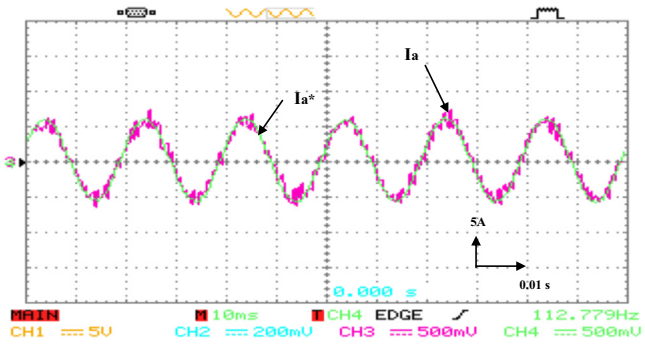

Fig. 19. Grid current with its reference.

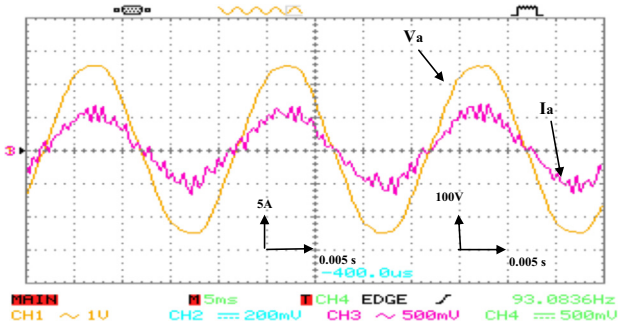

Fig. 20. Grid voltage and current curves.

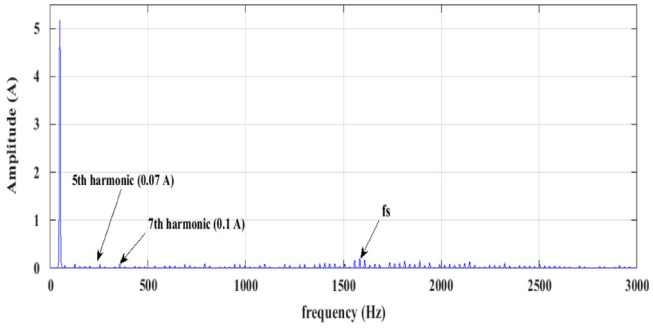

Fig. 21. Spectral analysis of the grid current.

subject to continuous adjustment, and very often, the gains obtained analytically or by simulation do not work well in practice. There are several causes for this: floating of PI parameters with the change in external conditions, saturation, noise, delays and imperfections in signal acquisition:

$$I_{\max} = PI(e) + I_{PVs} \tag{29}$$

Finally, Figs. 19 and 20 show the system performances on the grid side.

– From these figures, the expected performances obtained in the simulation step are approved, either in current tracking or in a total flow of the extracted PV power to the grid. Such performances can be used to improve the voltage quality in the grid nods, in case of deep voltages.

In Fig. 21 is displayed the harmonic analysis of the grid current. As remarked, no significant low order harmonics are noticed (5th and 7th); and the spectral content is affected mainly by the high harmonic switching frequencies f_s, around 1.5 kHz, as a result of the current control of the VS inverter. Consequently, the obtained total harmonic distortion factor (THD), is lower than 5%, meaning compliance with IEEE-519-1992.

5. Conclusion

In this work, a real time implementation of a small scale grid connected photovoltaic system, based on both sliding mode and fuzzy logic control was presented. The various control techniques were tested through simulation and validated with experiment, providing similar performances. The sliding mode based MPPT controller provides a high efficiency, since it permits to track the optimum power quickly despite the atmosphere condition changing. Besides, the regulation of the DC link voltage based on fuzzy logic controller, and the current control of the VS inverter has allowed a unity power factor operation.

Appendix

1) Data of the PV array at STC conditions (sharp):
P_{PV}=350 W, I_{sc}=5.4 A, V_{oc}=88.8 V, I_{op}=4.95 A, V_{op}=70.8 V.

2) Passive filters:
   $C=1100\mu F$, $L=10$ mH
3) Controllers parameters:
   - Sliding mode gain: $K=0.003$
   - FLC gains:$K_{11}=0.001$; $K_{12}=0.01$; $K_{13}=-60$.
   - PI gains: $K_p=0.5$,$K_i=1$
   - Hysterisis band: $\Delta i=0.01$
   - PLL function:

$$F_1(u)=V_\alpha \cos(\theta)+V_\beta \sin(\theta)$$

$$F_2(u)=V_\beta \cos(\theta)-V_\alpha \sin(\theta)$$

References

[1] Posadillo R, López Luque R. Approaches for developing a sizing method for stand-alone PV systems with variable demand. Renew Energy 2008;33:1037–48.
[2] Fragaki A, Markvart T. Stand-alone PV, system design: results using a new sizing approach. Renew Energy 2008;33:162–7.
[3] Casaro MM, Martins DC. Behavior matching technique applied to a three-phase grid-connected PV system. In: Proceedings of IEEE international conference on sustainable energy technologies, ICSET; 2008. p. 12–17.
[4] Notton G, Lazarov V, Stoyanov L. Optimal sizing of a grid-connected PV system for various PV module technologies and inclinations, inverter efficiency characteristics and locations. Renew Energy 2010;35:541–54.
[5] Li S, Attou A, Yang Y, Geng D. A maximum power point tracking control strategy with variable weather parameters for photovoltaic systems with DC bus. Renew Energy 2015;74:478–88.
[6] D'Souza NS, Lopes LA, Liu X. Comparative study of variable size perturbation and observation maximum power point trackers for PV systems. Electr Power Syst Res 2010;80:296–305.
[7] Kakosimos PE, Kladas AG. Implementation of photovoltaic array MPPT through fixed step predictive control technique. Renew Energy 2011;36:2508–14.
[8] Algazar MM, Al-Monier H, EL-halim HA, Salem MEEK. Maximum power point tracking using fuzzy logic control. Int J Electr Power Energy Syst 2012;39:21–8.
[9] Ezzat Salem M. Maximum power point tracking using fuzzy logic control; 2004.
[10] Shaiek Y, Ben Smida M, Sakly A, Mimouni MF. Comparison between conventional methods and GA approach for maximum power point tracking of shaded solar PV generators. Sol Energy 2013;90:107–22.
[11] Larbes C, Ait Cheikh S, Obeidi T, Zerguerras A. Genetic algorithms optimized fuzzy logic control for the maximum power point tracking in photovoltaic system. Renew Energy 2009;34:2093–100.
[12] Sa-ngawong N, Ngamroo I. Intelligent photovoltaic farms for robust frequency stabilization in multi-area interconnected power system based on PSO-based optimal Sugeno fuzzy logic control. Renew Energy 2015;74:555–67.
[13] Chaouachi A, Kamel RM, Nagasaka K. A novel multi-model neuro-fuzzy-based MPPT for three-phase grid-connected photovoltaic system. Sol Energy 2010;84:2219–29.
[14] Mohd Zainuri M, Radzi M, Soh AC, Rahim NA. Adaptive P&O-fuzzy control MPPT for PV boost DC–DC converter. In: Proceedings of IEEE international conference on power and energy; 2012. p. 524–9.
[15] Betka A, Attali A. Optimization of a photovoltaic pumping system based on the optimal control theory. Sol Energy 2010;84:1273–83.
[16] Marouani R, Mami A. Voltage oriented control applied to a grid connected photovoltaic system with maximum power point tracking technique. Am J Appl Sci 2010;7:1168.
[17] Kim I-S, Kim M-B, Youn M-J. New maximum power point tracker using sliding-mode observer for estimation of solar array current in the grid-connected photovoltaic system. IEEE Trans Ind Electron 2006;53:1027–35.
[18] Rekioua D, Achour A, Rekioua T. Tracking power photovoltaic system with sliding mode control strategy. Energy Procedia 2013;36:219–30.
[19] Slotine J-JE, Li W. Applied nonlinear control. 3rd ed., Addison Wesley; 2005.
[20] Chu C-C, Chen C-L. Robust maximum power point tracking method for photovoltaic cells: a sliding mode control approach. Sol. Energy 2009;83:1370–8.
[21] Hamrouni N, Jraidi M, Cherif A. New control strategy for 2-stage grid-connected photovoltaic power system. Renew Energy 2008;33:2212–21.
[22] Won C-Y, Kim D-H, Kim S-C, Kim W-S, Kim H-S, A new maximum power point tracker of photovoltaic arrays using fuzzy controller. In: Proceedings of the 25th annual IEEE conference record on power electronics specialists, PESC; 1994. p. 396–403.
[23] Matsui M, Kitano T, Xu D. A simple maximum photovoltaic power tracking technique utilizing system inherent limit cycle phenomena. In: Proceedings of the 38th IAS annual meeting conference record of the industry applications conference; 2003. p. 2041–7.
[24] Guerrero-Rodríguez N, Herrero-de Lucas L, de Pablo-Gómez S, Rey-Boué AB. Performance study of a synchronization algorithm for a 3-phase photovoltaic grid-connected system under harmonic distortions and unbalances. Electr Power Syst Res 2014;116:252–65.